14th International Symposium on Particle Image Velocimetry – ISPIV 2021
August 1–5, 2021

Volumetric velocimetry for small seeding tracers in large volumes

Y. Zhang[1*], H. Abitan[1], S. L. Ribergård[1], C. M. Velte[1]

[1] Technical University of Denmark, Department of Mechanical Engineering, Kgs. Lyngby, Denmark

[*] yiszh@mek.dtu.dk

Abstract

This paper presents the volumetric velocity measurement method of small seeding tracer with diameter $5\mu m \sim 100\mu m$ for volumes of $\geq 500cm^3$. The size of seeding tracer is between helium-filled soap bubbles (HFSB) and di-ethyl-hexyl-sebacic acid ester(DEHS) droplets. The targeted measurement volume dimension is equivalent to the volume of HFSB, which will give a higher resolution of turbulence study. The relations between particle size, imaging and light intensity are formulated. The estimation of the imaging results is computed for the setup design. Finally, the methodology is demonstrated for turbulence velocity measurements in the jet flow, in which the velocities of averaged diameter $15\mu m$ air filled soap bubbles are measured in a volume of $7200cm^3$.

1 Introduction

There is a strong push for large volumetric velocity measurement using small tracers in Barros et al. (2021). Normally, due to light scattering and characterics length scale considerations, big tracers are used for tracing large eddies in big volumes, and smaller tracers are applied for microscale eddies in smaller volumes. As can be expected from Figure 1, there is a noticeable gap between attainable volumetric domains for large ($\geq 300cm^3$) and small ($1\mu m \sim 20\mu m$) tracers in the range between $10^2\,cm^3 \sim 10^4\,cm^3$.

As part of a long-term combined theoretical and experimental initiative, we are setting out to experimentally test the degree of locality of the interactions between wavenumber components. This requires measurements that cover the 'global' dynamics of the flow, while also capturing as wide a bandwidth of the turbulent (temporal and spatial) spectrum as possible. Soap bubbles of diameter $\sim 15\mu m$ can follow the flow accurately to the degree of spatio-temporal resolution in the experimental design while at the same time they are highly resilient and long-lived and therefore the most viable option from a practical point of view. Therefore, these smaller seeding particles are the key factor to these experiments.

Discetti and Coletti (2018) summarized methods that have been developed to measure the full volumetric velocity (3D–3C, i.e. three-dimensional and three-component). In the past two decades, volumetric velocimetry has evolved from experiments at moderate scale of $10\,cm^3$ up to large scales of $10^4\,cm^3$ by various experiments. The initial tomo-PIV experiment done by Elsinga et al. (2006) was conducted with $1\mu m$ droplets in a volume of $13\,cm^3$. Later the larger measurement volumes were obtained by volumetric velocimetry in air conducted by Schröder et al. (2009), Humble et al. (2009), Violato et al. (2011), Ghaemi and Scarano (2011), Schröder et al. (2011) and Atkinson et al. (2011), which did not exceed $10^2\,cm^3$ measurement volume with micron-scale seeding tracers.

The main factors limiting the scale up of PIV to macroscopic dimensions summarized by Scarano et al. (2015) are the limited illumination energy from the illumination source, the scattering efficiency of the tracers, the small optical aperture (due to large depth of field), and the sensitivity and spatial resolution of the camera sensors. With low repetition rate (prolonging exposure time) and millimeter scale HFSB (increasing scattering efficiency), larger measurement volumes can be observed to characterize large scale flow structure in the experiments of Lobutova et al. (2009) and Kühn et al. (2011).

For turbulent flows, the inherent instability and three dimensions requires high resolution time-resolved volumetric velocimetry. It is impossible to utilize millimeter scale tracers to measure the same scale turbulent structure, because the length scale of the structure is smaller than the tracer diameter, and the cut-off

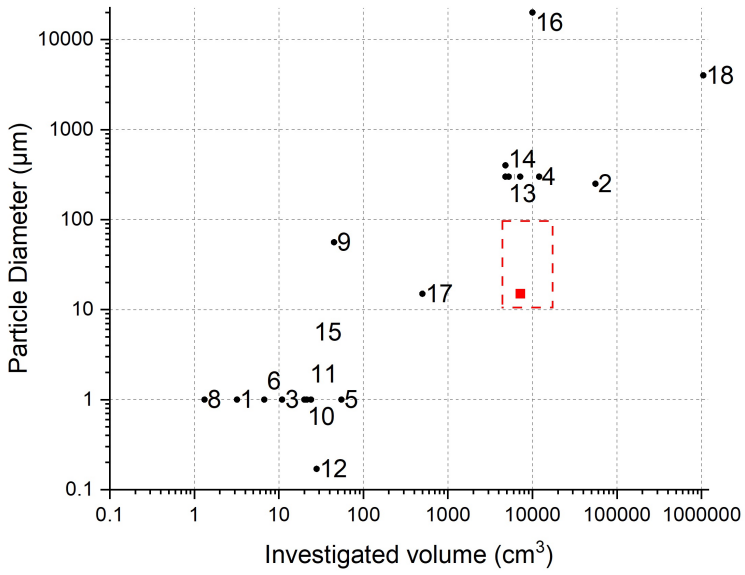

Figure 1: Compilation of volumetric velocimetry investigations in air flows: the particle diameter and the imaged volume. The labeled points refers to the researches in the references: 1, Atkinson et al. (2011); 2, Kühn et al. (2011); 3,Cafiero et al. (2015); 4, Caridi et al. (2016); 5, Boushaki et al. (2017); 6, Pröbsting et al. (2013); 7, Schneiders et al. (2016); 8,Schneiders and Scarano (2016); 9, Schneiders and Scarano (2016); 10, Elsinga et al. (2006); 11, Schröder et al. (2007); 12, Humble et al. (2009); 13, Terra et al. (2017); 14, Scarano et al. (2015); 15, Michaelis et al. (2012); 16, Hou et al. (2021); 17, Barros et al. (2021); 18, Bosbach et al. (2009). The red square is the current study and the red area is the interested study area.

diameter of the particles deduced from cut-off frequency could be micron-scale (see Mei (1996)). The current investigation aims at characterizing both the 'global' flow structure and millimeter scale structure with micron-scale tracers.

With the capabilities of low resolution cameras,, the only option to capture the turbulence structure is to observe small tracers in a small measurement volume. Now with the development of camera sensor techniques, the high resolution cameras in recent years provide the possibility of capturing the intermediate-size turbulence structure in a larger volume, in which the whole evolution process of the turbulent spectrum can be observed. However, there is still a problem between the visibility of seeding tracers and the following effect of intermediate-size turbulence structure. In order to visualize small structures in the turbulence flow, micron-scale tracers are needed to follow the unstable and three dimensional millimetre scale structures. And as the result of reducing the tracer dimension, the signal from seeding tracers to camera would drop in quadratic proportion.

For the purpose of solving this problem, this paper thus details the computation of particle image size with tracers, lens and camera parameters. Then with the desired turbulent scales, the relation among camera, light source and measurement volume is formulated to make sure that the particle images cannot travel across pixels (to avoid streaky particle images). Two examples of approximate $15\mu m$ particles in a $7200\,cm^3$ volume, that are 10 times larger than Barros et al. (2021), are demonstrated at an acquisition frequency of $\sim 2KHz$. The current work thus documents how to design a time-resolved volumetric velocimetry experiment in a manner that the gap of smaller seeding particles for the target turbulent micro-scale structure in big volume for 'global' flow is filled.

The paper is organized as follows. In the Section 2, the methodology that related from flow characteristics, seeding, illumination and imaging was formulated. To demonstrate the computation, a jet flow example was computed in Section 3, where we use the all the formulas in Section 2. The setup and experiment result corresponding to the computation in Section 3 was provided in Section 4. Finally, our conclusion and perspectives are presented.

2 Methodology

2.1 Flow characteristics

The target smallest structure in the flow is characterized with length-scale ℓ and characteristic velocity $u(\ell)$. The timescale of these structure (see Pope (2000)) is:

$$\tau(\ell) \equiv \frac{\ell}{u(\ell)}. \tag{1}$$

Based on the timescale, the interested frequency is

$$f_i = \frac{1}{\tau(\ell)}. \tag{2}$$

According to the Shannon's sampling theorem, the camera minimum repetition rate f_c should be more than twice of the interested frequency $f_c \geq 2f_i$. Both the spatial resolution and the camera repetition are based on the flow length-scale and timescale.

2.2 Seeding

There are six factors that affects the particles to follow the flow from the study of Mei (1996), Adrian and Westerweel (2011) and Raffel et al. (2018). Response time and Stokes number are related to the fidelity of tracer particles accurately following the flow. Response time (τ_t) represents the characteristic time required for a tracer particle to reach an equilibrium condition after a flow disturbance. The response time is commonly calculated using the following form

$$\tau_t = d_p^2 \frac{\rho_p}{18\nu} \tag{3}$$

where d_p is the particle diameter, ρ_p is the particle density and ν is the kinematic viscosity of the ambient fluid. The Stokes number (Sk) is defined as the ratio of the characteristic time of a particle to a characteristic time of the flow (τ_f),

$$Sk = \frac{\tau_t}{\tau_f} \tag{4}$$

Because the smallest eddies are characterized the timescale $\tau(\ell)$, the flow characteristic time equals to the timescale $\tau_f = \tau(\ell)$. In general, a Stokes number of 0.1 or less given by Tropea et al. (2007) could return an acceptable flow tracing accuracy with errors below 1%.
In dynamic conditions like turbulent flows studied by Mei (1996), the particle frequency response function H_p that is defined as the sinusoidal response of particle to a sinusoidal oscillation of the flow relates to the bias between the particle velocity and flow velocity,

$$\hat{v}(\omega) = H_p(\omega)\hat{u}(\omega) \tag{5}$$

where $\hat{v}(\omega)$ is the particle velocity amplitude at frequency ω, and $\hat{u}(\omega)$ is the flow velocity amplitude, both of which are deduced from particle oscillation function $v(t) = \hat{v}(\omega)e^{-i\omega t}$ and flow oscillation function $u(t) = \hat{u}(\omega)e^{-i\omega t}$.
Defining Stokes number in frequency domain ε with the frequency variable ω (see Mei (1996)),

$$\varepsilon = \sqrt{\frac{\omega d_p^2}{2\nu}}, \tag{6}$$

the energy transfer function deduced from the particle frequency response function is

$$|H_p(\omega)| = |H_p(\varepsilon)| = \frac{(1+\varepsilon)^2 + (\varepsilon + \frac{2}{3}\varepsilon^2)^4}{(1+\varepsilon)^2 + [\varepsilon + \frac{2}{3}\varepsilon^2 + \frac{4}{9}(\rho-1)\varepsilon^2]^2}. \tag{7}$$

where, ρ is the density ratio of particles and ambient flow $\rho = \rho_p/\rho_f$, and ρ_f is the density of the ambient flow.
In the study of Mei (1996), the cut-off frequencies of the particles are based the 50% and 200% energy response, which means that $0.5 < |H_p(\omega)|^2 < 2$ implies very good response of the seeding particles. So the cut-off frequencies f_{cutoff}, the cut-off Stokes number ε_{cutoff} and the cut-off particle diameter d_{cutoff} can be computed from the follow equations:

$$\begin{cases} \varepsilon_{cutoff} = \{\varepsilon : |H_p(\omega)|^2 = 0.5 \text{ or } 2\} \\ \varepsilon_{cutoff} \approx [2.380^{0.93} + \left(\frac{0.659}{0.561-\rho} - 1.175\right)^{0.93}]^{\frac{1}{0.93}}, \text{ for } \rho < 0.561 \\ \varepsilon_{cutoff} \approx [\left(\frac{3}{2\rho^{1/2}}\right)^{1.05} + \left(\frac{0.932}{\rho-1.621}\right)^{1.05}]^{\frac{1}{1.05}}, \text{ for } \rho > 1.621 \\ f_{cutoff} \approx \frac{\nu}{\pi}\left(\frac{\varepsilon_{cutoff}}{d_p}\right)^2 \\ d_{cutoff} \approx \varepsilon_{cutoff}\sqrt{\frac{\pi f_{cutoff}}{\nu}} \end{cases} \tag{8}$$

However, in practice the computation process is the reversed version: a. find the particle parameter like diameter d_p and density ρ_p; b. compute the density ratio ρ and Stokes frequency domain number ε; c. get the energy transfer function result $|H_p(\omega)|^2$ and decide if the seeding type is suitable for the flow; d. compute the cut-off frequency to see if it can cover the interested frequency range.
To emphasize the unit of the parameters in the equations, kinematic viscosity in the equation 8 and 6 is expressed in terms of cm^2/s, and the diameter of particles is in the term of μm.

2.3 Imaging

The observed volume $V = L \times H \times W$ is imaged by cameras with the fixed optical magnification based on the sensor size. Defining the pixel resolution l_s, pixel pitch Δ_{pix}, and aperture number f_s, the optical magnification of the imaging system can be deduced from the ratio of the focal lens to the working distance.

$$M = \frac{l_s \Delta_{pix}}{L} = \frac{d_i}{d_o}. \tag{9}$$

Where d_o is the distance from the object geometrical center to the lens center and d_i is the distance from the image geometrical center to the lens center. The particle image τ_p on camera sensor can be computed from:

$$\tau_p = \frac{\sqrt{d_{op}^2 + d_s^2 + d_f^2}}{\Delta_{pix}} \tag{10}$$

where $d_{op} = M d_p$ is the particle diameter; d_s is diffraction limit spot diameter, which can be computed with aperture stop number f_s and light wave length λ by $d_s = 2.44(1+M)f_s\lambda$; and d_f is the blur circle diameter. The depth of focus (DOF) δ_z is

$$\delta_z = 2 d_s f_s \frac{1+M}{M^2} = 4.88 f_s^2 \lambda \frac{(1+M)^2}{M^2} \tag{11}$$

2.4 Scattered Light

In the PIV experiment, part of the incident light is scattered by the tracers onto the camera sensors. The light scattering properties of a homogeneous and isotropic sphere in a plane wave, which leads to the Lorenz-Mie Theory, are well documented in van de Hulst (1981), thus only related final results are presented to obtain the light source budget.
The first step is to project the incident wave vector onto the scattering plane. From camera lens, the received electric field vector can be expressed as

$$\mathbf{E}_r = \frac{e^{-i\mathbf{k}_\omega \mathbf{r}_p}}{\mathbf{k}_\omega \mathbf{r}_p} \mathbf{M}_\beta \mathbf{M}_S \mathbf{M}_\varphi \mathbf{E}_0 \tag{12}$$

where $\mathbf{E}_0$ is incident plane wave vector, $\mathbf{k}_\omega$ is the incident wave vector, and $\mathbf{r}_p$ is the scattering vector between the particle center and lens center, the angle between $\mathbf{k}_\omega$ and $\mathbf{r}_p$ is ϑ, the scattering plane lies at an angle of φ, $\mathbf{M}_S$ is the scattering matrix with sum of scattering functions, $\mathbf{M}_\beta$, and $\mathbf{M}_\varphi$ is plan transform matrix (details to see Albrecht et al. (2003) pages:79-126).
One dimensionless parameter defined as Mie parameters is important to the scattering intensity,

$$x_M = \frac{\pi d_p}{\lambda}. \tag{13}$$

For particles with Mie parameter $x_M > 10$, the scattered intensity increases with the second power of the particle diameter, which means geometrical optics can be applied for approximate computation. For the Lorenz-Mie region with $1 \leq x_M \leq 10$, the scattered intensity exhibits strong oscillations. The received light intensity is

$$I_r(\lambda, r, \vartheta) = \frac{c\varepsilon}{2}|\mathbf{E}_0|^2 \tag{14}$$

where ε is the permittivity of the medium, c is the speed of light.
The photons signal I_c received by the cameras is the inner product of the light intensity distribution function and the camera sensor quantum efficiency function $\Phi_{qe}(\lambda)$,

$$I_c = \int\int \Phi_{qe}(\lambda) I_r(\lambda, r, \vartheta) d\lambda dA. \tag{15}$$

The integral of the area depends on the aperture diameter. If the distance between particle and lens is much larger than the efficient aperture $r \gg D$ and the scattering angle is in the range of geometrical optics, the scattering angle can be consider as constant. Thus the integral is only the constant intensity multiply the efficient aperture area.
The signal-to-noise ratio *SNR* in this paper follows the definition of Scharnowski and Kahler (2016), which used standard deviations of the image intensity and the noise:

$$SNR = \frac{\sigma_A}{\sigma_n}, \tag{16}$$

where σ_n is the standard deviation of the noise level, and σ_A is the standard deviation of the signal level, which can be approximated with number particle images per pixel N_{ppp},

$$\sigma_A = \frac{I_c}{2}\sqrt{N_{ppp} \cdot (\frac{\pi}{4}\tau_p^2 - 1)} \tag{17}$$

The loss-of-correlation due to image noise F_σ is defined as,

$$F_\sigma = \frac{\sigma_A^2}{\sigma_A^2 + \sigma_n^2} = \big(1 + \frac{1}{SNR^2}\big)^{-1}. \tag{18}$$

Before experiments start, the noise level σ_n can be estimated from the camera manuals. From the theory analysis and experimental evaluation in Scharnowski and Kahler (2016), the loss-of-correlation F_σ increase strongly from 0.4 to 0.8 with linearly increment of light power. So the main focus of the light design is to pursuit the higher F_σ below 0.8 under the limited light source budget.

3 Measurement computation in a jet flow example

In this section, we demonstrate the computation process of the visibility problem in a jet flow with approximate $15\mu m$ diameter air-filled bubbles in a volume of $30cm \times 30cm \times 8cm$. The whole estimation is carried out under the condition of International Standard Atmosphere (ISA).

3.1 Axisymmetric jet flow

The axisymmetric jet flow is one of the best canonical flow for understanding the turbulence. It has been interrogated using both experimental and theoretical methods. We model the jet velocity field based on the experimental investigation results by Hussein et al. (1994).
According to measurement result in Buchhave and Velte (2017), for 1 cm jet at $Re = 19868$, the length Taylor microscales are $2.2mm$ and the temporal Taylor microscales are $1ms$ at the center line at $30D$ downstream location and , which requires particle cut-off frequency higher than $1KHz$ and camera repetition rate higher than $2KHz$. From 13mm radial distance off the jet centerline, the temporal Taylor microscales are $2ms$, which requires particle cut-off frequency $500Hz$.

3.2 Seeding computation

The seeding tracers that we use to verify the method are the air-filled micron-scale bubble tracers, which have mean diameters of approximately $15\mu m$. Barros et al. (2021) investigated the characteristics of the seeding in a wind tunnel experiment. The theoretical response time computed from equation 3 is $20\mu s$, and the measured mean response time was $40\mu s$. More details of the microbubble tracer and the bubble generator can be found in Barros et al. (2021).
The reason we choose this type of seeding is that the tracers size is big enough to reflect light signal, and is small enough to show trajectory of Taylor micro-scale, and the response time is small enough to follow Taylor micro-scales. As the temporal Taylor micro-scales measured by Buchhave and Velte (2017) is $1ms$ at the center line at 30D downstream location for 1 cm jet at $Re = 19868$, the Stokes number of the micro-bubbles was found to be 0.04, which is in the acceptable upper limit of 0.1 given by Tropea et al. (2007).
According to Kerho and Bragg (1994) and Afanasyev et al. (2011), the wall thickness of soap bubbles lies in the range $0.1\mu m \sim 0.3\mu m$, the density of the bubbles is $20 \sim 70 kg \cdot m^{-3}$ in Barros et al. (2021). Taking the visible bubble diameter from $10\mu m \sim 30\mu m$, which have the frequency domain Stoke number at 0.26 and 0.47, the cut-off frequencies varies from $752.2Hz$ for large high density bubbles to $6.77KHz$ for small low density bubbles. And the mean cut-off frequency is 2.21KHz for $15\mu m$ particles with $0.2\mu m$ wall thickness. So in the radial range of $13mm$ at 30D downstream, only minor parts of the tracers (2.5% computed from statistics in Barros et al. (2021)), of which the diameter is larger than $30\mu m$ and the wall thickness is thicker than $0.3\mu m$, cannot represent the Taylor microscale in the $10mm$ jet. Out the radial range of $13mm$ at $30D$ downstream, all the tracers follows the Taylor microscale eddies well. For the average diameter particles, the energy transfer function in equation 7 equals to 0.7088, which is in the efficient response range.

3.3 Imaging computation

Considering the sensor size $27.6mm \times 26.3mm$ with resolution 2048 × 1944px and pixel pitch $13.5\mu m$, the magnification is 0.0875. Only computing the aperture number with $\lambda = 625$ that is the highest quantum efficient point of the camera used in the Section 4.2, the aperture number 13 is as DOF=8cm. So the F-stop is set at 16 due to the discrete number. The particle image τ_p is 1.97. To avoid to interfere the flow, the lens and the jet nozzle are in the same plane parallel to the front plane of the investigated volume, thus the distance from the object geometrical center to the lens center d_o is $35cm$ with the camera angle at 30°. So the focal length f is 28.16mm. The 35mm lens is adapted due to discrete product models.

3.4 Light budget computation

The emission spectra of a white light LED consists of a wide wavelength band from 440-760 nm. In order to simplify the estimation of the image signal, we consider the optical power as if it is emitted at the single wavelength $\lambda = 625nm$. i.e. the following computation is based on $\lambda = 625\,nm$ and corresponding photon energy of 3.2×10^{-19} Joules. At this wavelength the Mie parameters x_M equals 75.4, which is in the range of geometrical optics approximate computation. At the scattering angle of 90°, the light brightness at the target is 10^6 lux per LED. The averaged Mie scattering coefficient is about $8.6 \times 10^{-12} m^{-2}$. The received light energy of the CMOS detector is 2.95×10^{-18} Joules. The quantum efficiency of the CMOS detector of the camera at this photon energy is 0.95.
Plugging these parameters into the aforementioned model for estimating, the signal from one particle gives 8.8 counts for one LED set. If a LED can be pivoted to the cameras for acquiring a better scattering angle like , for example, 75°, the received light energy would be 1.39×10^{-17} Joules, and the particle signal on

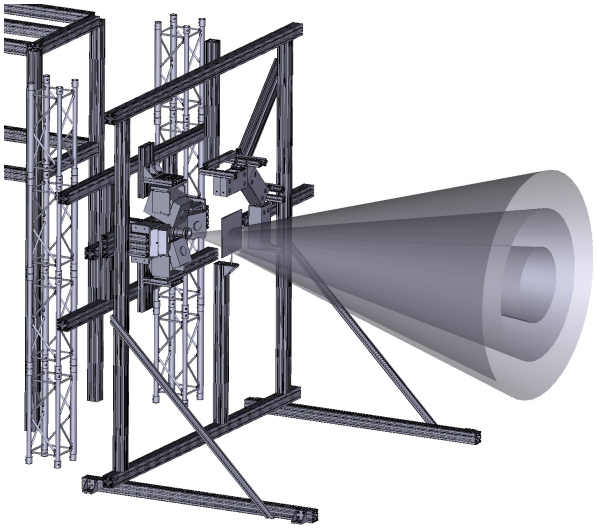

(a) Drawing of the current FF setup (preliminary).

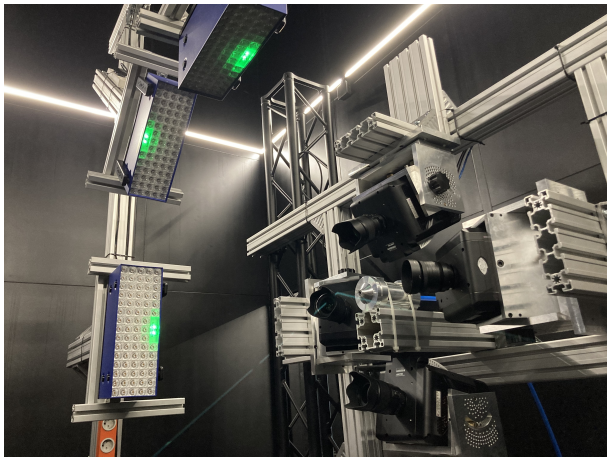

(b) Drawing of the current FF setup (preliminary).

Figure 2: The current setup in the Full Field section in Turbulence Research Laboratory at Technical University of Denmark.

the sensor is about 41.6 counts for each LED set. The noise level of the CMOS detector is $\sigma_n = 7.2$, the signal level is 10.8 and the required light density I_c is 148 counts with assuming $N_{ppp} = 0.01$. So the number of required LED sets is 3.5. Because all the computation are conserved, we choose to use 3 LEDs in the experiment.

4 Experiment and results

Experiments are conducted in a facility of the Turbulence Research Laboratory (TRL) of the Department of Mechanical Engineering at Technical University of Denmark. The TRL consists of two separate test cells – the High-Resolution experiment test cell and the Full-Field (FF) experiment test cell (see Ribergaard et al. (2021)). The experiment in this paper are implemented in the Full-Field testcell.

4.1 Jet facility

In the Full-Field test cell, a jet with 10mm diameter nozzle was placed in the center of injection wall. At the end of jet downstream direction, a sucking plate was mounted on the wall. The whole Full-Field test cell has a volume of 4600mm (streamwise length) ×4010mm (width) ×4930mm (height). Outside of the test section, there is an air recirculation controlling the air flow and the seeding density without influencing flow in the test cell.

4.2 Camera

The visualization system that we used is a commercial LaVision PIV/PTV system, which consists of four 2048 × 1944px CMOS high-speed video cameras (v2640), a Programmable Timing Unit(PTU) and system software Davis10. The sensor size is $27.6mm \times 26.3mm$, and the pixel pitch is $13.5\mu m$ with 12-bit depth. The cameras were arranged symmetrically facing the volume of interest(VOI), as shown in Figure 2(b). The cameras were angled at $\alpha = 30^\circ$ to the jet center line. The cameras were mounted on a 4 degree of freedom frame, which help to adjust the view angle at the minimum point independently. According to computation from Section 3, the lens focal length is 35mm, and the aperture is set at f# 8.

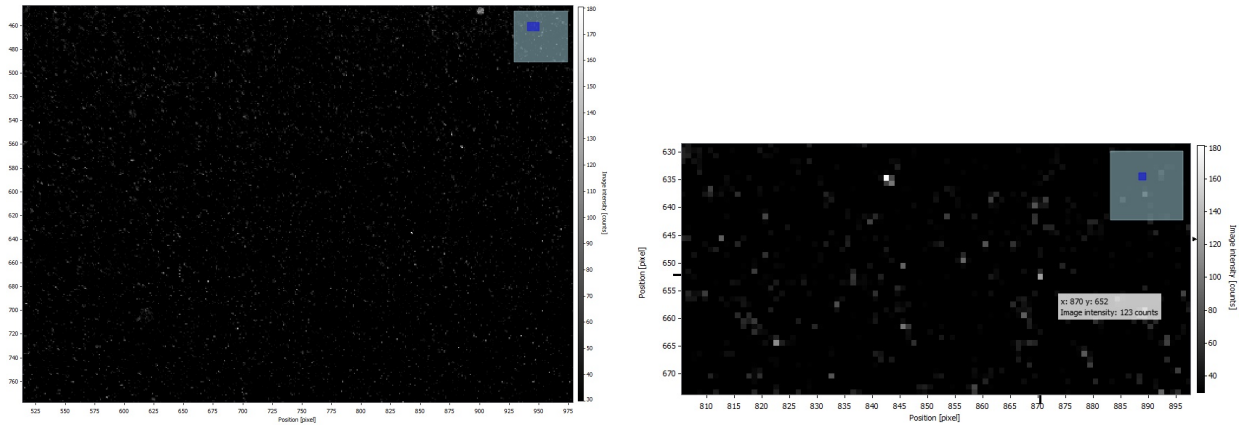

(a) The sub-image of the measurement.

(b) The signal intensity is 80-160 counts.

Figure 3: A sample image acquired from one camera.

4.3 Lights

The light sources we use in the experiment are an array of Flashlight 300 LEDs, which is produced by LaVision GmbH. These high power LEDs consist of 72 diodes each. The opening angle is 10°. In the pulsed-overdrive mode, the LEDs are operated above the nominal LED current to generate short pulses at about 5 times high light intensities than the free trigger mode. but to protect the LEDs at such high current, the duty cycle is limited to a maximum of 10%. The brightness can be measured above 10^6 lux at 1m distance.
In order to acquire better light conditions, forward scattering is applied by rotating the LEDs to the camera.

4.4 Bubble generator

The air-filled soap bubble generator used in this paper was developed by TSI and had been applied for several wind tunnel experiements. It consists of a 57 liter reservoir filled with a 5% surfactant-water solution. The surfactant was common non-color and non-perfume pure dish-washing detergent. At bottom of the reservoir, a piston pump is used to draw and pressurize the solution through a high pressure tube with a set of 10 nozzles. The outlet diameter of the nozzles is 0.2mm, and could be blocked with special blank nozzle heads to reduce the seeding generating rate.
The air-filled-soap-bubble tracers have mean diameter of 14.7μm, response time 40μs with a dispersion of 30μm. The bubbles can be generated at high rates of 50 tracers per cm^3. The Stokes number of the micro-bubbles was 0.04, which could show the flow trajectory faithfully.

4.5 Result

For each snapshot, the number of the traced particles was in the range 7000–9000. A sample image acquired by one camera was shown in Fig. 3(a), in which the particles can be clearly identified by the LaVison Davis system. The particle size is 2-4 pixels, in agreement with computation. As shown in Fig. 3(b), the signal intensity from the camera sensor is about 80-160 counts, which is in the same level with the estimated 147 counts in section 3. The main difference may be due to the different angle of LED to different cameras.

5 Conclusions

To cover the whole range from the global eddies to the smallest interested eddies, the relations of particle size, imaging, light intensity are formulated. From the characteristic timescale and length scale of the smallest interested eddies, the tracer type can be chosen by the diameter and density. Then the light intensity can be estimated from the particle and the necessary minimum distance of the setup. With all the computed parameters, one setup for jet flow measurement was prepared for the volumetric velocimetry in the volume

of $\geq 5000\,cm^3$. The selected seeding tracer is air-filled soap bubbles with diameter of approximately $15\mu m$, of which the size of seeding tracer is between millimeter scale HFSB and $1\mu m$ scale DEHS. The targeted measurement volume dimension is equivalent to the volume of HFSB, which will give a higher resolution of turbulence study. The evaluation method in Section 2 can successfully predict the visibility of the small tracers.
Our furthur work is to observe Taylor micro-scale in the same time to catch the global eddies at $Re = 15 \times 10^3$ in the 1 cm jet flow. A higher Reynolds number is possible to be achieved with well designed illumination source.

Acknowledgements

This project has received funding from the European Research Council (ERC) under the European Unions Horizon 2020 research and innovation program (grant agreement No 803419). The Department of Mechanical Engineering at the Technical University of Denmark is also acknowledged for their generous additional support in establishing the laboratory.

References

Adrian RJ and Westerweel J (2011) *Particle image velocimetry*. Cambridge University Press

Afanasyev Y, Andrews G, and Deacon C (2011) Measuring soap bubble thickness with color matching. *American Journal of Physics* 79:1079–1082

Albrecht H, Borys M, Damaschke N, and Tropea c (2003) *Laser Doppler and Phase Doppler Measurement Techniques*. Springer-Verlag Berlin Heidelberg

Atkinson C, Coudert S, Foucaut J, Stanislas M, and Soria J (2011) The accuracy of tomographic particle image velocimetry for measurements of a turbulent boundary layer. *Experiments in Fluids* 50:1031–1056

Barros DC, Duan Y, Troolin DR, and Longmire EK (2021) Air-filled soap bubbles for volumetric velocity measurements. *Experiments in Fluids* 62

Bosbach J, Kühn M, and Wagner C (2009) Volumetric velocity measurements (v3v) on turbulent swirling flows. *Experiments in Fluids* 46:539–547

Boushaki T, Koched A, Mansouri Z, and Lespinasse F (2017) Volumetric velocity measurements (v3v) on turbulent swirling flows. *Flow Meas Instrum 54:46–55* 54:46–55

Buchhave P and Velte CM (2017) Measurement of turbulent spatial structure and kinetic energy spectrum by exact temporal-to-spatial mapping. *PhysFluids* 29:085109

Cafiero G, Discetti S, and Astarita T (2015) Flow field topology of submerged jets with fractal generated turbulence. *Phys Fluids* 27:115

Caridi G, Ragni D, Sciacchitano A, and Scarano F (2016) Hfsb-seeding for large-scale tomographic piv in wind tunnels. *Experiments in Fluids* 52:190

Discetti S and Coletti F (2018) Volumetric velocimetry for fluid flows. *Meas Sci Technol* 29

Elsinga G, Scarano F, Wieneke B, and van Oudheusden B (2006) Tomographic particle image velocimetry. *Experiments in Fluids* 41:933–947

Ghaemi S and Scarano F (2011) Counter-hairpin vortices in the turbulent wake of a sharp trailing edge. *Journal of Fluid Mechanics* 689:317–356

Hou J, Kaiser F, Sciacchitano A, and Rival DE (2021) A novel single-camera approach to large-scale, three-dimensional particle tracking based on glare-point spacing. *Experiments in Fluids* 63

Humble R, Elsinga G, Scarano F, and Van Oudheusden B (2009) Three dimensional instantaneous structure of a shock wave/turbulent boundary layer interaction. *Journal of Fluid Mechanics* 622:33–62

Hussein H, Capp S, and George W (1994) Velocity measurements in a high-reynolds-number, momentum-conserving, axisymmetric, turbulent jet. *Journal of Fluid Mechanics* 285:31–75

Kerho M and Bragg M (1994) Neutrally buoyant bubbles used as flow tracers in air. *Experiments in Fluids* 16:393–400

Kühn M, Ehrenfried K, Bosbach J, and Wagner C (2011) Large-scale tomographic particle image velocimetry using helium-filled soap bubbles. *Experiments in Fluids* 50:929–948

Lobutova E, Resagk C, Rank R, and Müller D (2009) *Extended three dimensional particle tracking velocimetry for large enclosures. In Imaging measurement methods for flow analysis*. Springer

Mei R (1996) Velocity fidelity of flow tracer particles. *Experiments in Fluids* 22:1–13

Michaelis D, Bomphrey R, Henningsson P, and Hollis D (2012) Reconstructing the vortex skeleton of the desert locust using phase averaged pod approximations from time resolved thin volume tomographic piv. in *16th International symposium on applications of laser techniques to fluid mechanics, Lisbon, Portugal*

Pope SB (2000) *Turbulent Flows*. Cambridge University Press

Pröbsting S, Scarano F, Bernardini M, and Pirozzoli S (2013) On the estimation of wall pressure coherence using time-resolved tomographic piv. *Experiments in Fluids* 54:1567

Raffel M, Willert C, Scarano F, Kähler C, Wereley S, and Kompenhans J (2018) *Particle Image Velocimetry: A Practical Guide Third Edition*. Springer International Publishing

Ribergaard S, Zhang Y, Abitan JS Hand Nielsen, Jensen N, and Velte C (2021) A novel laboratory pushing the limits for optics-based basic turbulence investigations. in *14th International Symposium on Particle Image Velocimetry- ISPIV 2021, Chicago, Illinois, USA, August 1-5*

Scarano F, Ghaemi S, Caridi G, Bosbach J, Dierksheide U, and Sciacchitano A (2015) On the use of helium-filled soap bubbles for large-scale tomographic piv in wind tunnel experiments. *Experiments in Fluids* 56

Scharnowski S and Kahler C (2016) On the loss-of-correlation due to piv image noise. *Experiments in Fluids* 57

Schneiders J, Caridi G, Sciacchitano A, and Scarano F (2016) Largescale volumetric pressure from tomographic ptv with hfsb tracers. *Experiments in Fluids* 57

Schneiders JF and Scarano F (2016) Dense velocity reconstruction from tomographic ptv with material derivatives. *Experiments in Fluids* 57

Schröder A, Geisler R, Elsinga G, Scarano F, and Dierksheide U (2007) Investigation of a turbulent spot and a tripped turbulent boundary layer flow using time-resolved tomographic piv. *Experiments in Fluids* 44:305–316

Schröder A, Geisler R, Sieverling A, Wieneke B, Henning A, Scarano F, Elsinga G, and Poelma C (2009) Lagrangian aspects of coherent structures in a turbulent boundary layer flow using tr-tomo piv and ftv. in *8th international symposium on particle image velocimetry*

Schröder A, Geisler R, Staack K, Elsinga G, Scarano F, Wieneke B, and Westerweel J (2011) Eulerian and lagrangian views of a turbulent boundary layer flow using time-resolved tomographic piv. *Experiments in Fluids* 50:1071–1091

Terra W, Sciacchitano A, and Scarano F (2017) Aerodynamic drag of a transiting sphere by large-scale tomographic-piv. *Experiments in Fluids* 58

Tropea C, Foss J, and Yarin A (2007) *Springer Handbook of Experimental Fluid Mechanics*. Springer

van de Hulst H (1981) *Light scattering by small particles*. Dover Publications

Violato D, Moore P, and Scarano F (2011) Lagrangian and eulerian pressure field evaluation of rod-airfoil flow from time-resolved tomographic piv. *Experiments in Fluids* 50:1057–1070